Evidence of Enhanced Ion Transport in Li-Rich Silicate Intercalation Materials

Juliette Billaud, Christopher Eames, Nuria Tapia-Ruiz, Matthew R. Roberts, Andrew J. Naylor, A. Robert Armstrong, M. Saiful Islam, and Peter G. Bruce**

The silicate compounds Li_2MSiO_4 (where M = Mn, Fe, Co) have received significant attention recently as Li intercalation electrodes. Overwhelmingly they exhibit relatively poor kinetics of ion intercalation. By synthesizing Li-rich solid solutions of the form $Li_{2+2x}Fe_{1-x}SiO_4$ (with $0 \le x \le 0.3$), the structural requirements for fast ion transport and hence relatively fast intercalation have been identified. Specifically the presence of additional Li^+ in interstitial sites, not normally occupied in the stoichiometric Li_2FeSiO_4 compound, enhances ion transport by more than two orders of magnitude. The results, obtained by combining electrochemical measurements, with powder X-ray and neutron diffraction and atomistic modeling of the ion dynamics, provide valuable guidance in designing future intercalation electrodes with high Li-ion transport and, hence, fast electrode kinetics.

1. Introduction

Polyoxyanion-type intercalation electrodes based on the orthosilicates, Li_2MSiO_4 (where M = Mn^{2+}, Fe^{2+}, Co^{2+}), have been attracting significant attention.[1–55] The major drawback of these materials is their poor rate performance, which is hindered by low lithium diffusion coefficients.[9,31–33] Before new materials with high host ion diffusivity and hence high electrode kinetics can be synthesized, it is first necessary to understand why the current materials are slow and what structural features control the ion diffusion.

Here we synthesize several $Li_{2+2x}Fe_{1-x}SiO_4$ samples, and demonstrate the presence of sites for interstitial lithium using neutron diffraction data. We show by electrochemical measurements and atomistic modeling studies that occupancy of these sites raises the Li^+ diffusivity by two to three orders of magnitude, significantly enhancing the electrode kinetics compared with those of stoichiometric Li_2FeSiO_4.

1.1. Structural Chemistry of Li_2MSiO_4

Li_2MSiO_4 compounds (where M = Mg, Zn, Mn, Co, Fe, and Cd) belong to the family of tetrahedral oxides. Their structures and extensive polymorphism have been described previously.[2,12,13] The orthosilicate structures consist of slightly distorted close-packed oxygen layers in between which cations occupy 50% of the tetrahedral sites. Within this general description there are two main structure types, denoted β and γ, corresponding to low and high temperature forms (**Table 1**). Structurally, these two compounds differ in the MO_4 tetrahedral arrangement; in the β-polymorph MO_4 tetrahedra point in the same direction, perpendicular to the close-packed oxygen planes, whereas for the γ type half of the MO_4 tetrahedra are inverted.

Li_2FeSiO_4 compounds prepared at 600–800 °C adopt a structure designated by Nishimura et al.[6] as γ_s (Table 1), which contains edge-sharing pairs of tetrahedra; one set of LiO_4 tetrahedra shares edges with FeO_4 tetrahedra, whilst the other set of LiO_4 tetrahedra forms edge-sharing pairs with itself (Table 1). By quenching from 900 °C a new γ_{II}-polymorph of Li_2FeSiO_4 may be obtained,[12] isostructural with Li_2CdSiO_4 (space group *Pmnb*, Table 1). In most γ structures, the tetrahedra are arranged in groups of three with the central tetrahedron pointing in the opposite direction to the outer two, with which it shares edges. In the case of the γ_{II} structure the group of three edge-sharing tetrahedra consists of a Li-M-Li sequence. This structure is adopted by $Li_{2+2x}Zn_{1-x}GeO_4$, which is a Li^+ conducting solid electrolyte (LISICON) (**Figure 1**). The interstitial Li^+ (in the octahedral sites and sharing two faces with the substituting Li^+) gives rise to the higher conductivity of the solid solution compared with stoichiometric Li_2ZnGeO_4.[56]

2. Results and Discussion

2.1. Structural Analysis

Powder X-ray diffraction patterns for the $Li_{2+2x}Fe_{1-x}SiO_4$ materials ($0 \le x \le 0.3$) are presented in **Figure 2**. Compositional

Dr. J. Billaud, Dr. A. R. Armstrong
School of Chemistry
University of St Andrews
St Andrews, Fife KY16 9ST, UK
Dr. C. Eames, Prof. M. S. Islam
Department of Chemistry
University of Bath
Bath BA2 7AY, UK
E-mail: M.S.Islam@bath.ac.uk
Dr. N. Tapia-Ruiz, Dr. M. R. Roberts, Dr. A. J. Naylor, Prof. P. G. Bruce
Department of Materials and Chemistry
University of Oxford
Oxford OX1 3PH, UK
E-mail: peter.bruce@materials.ox.ac.uk

DOI: 10.1002/aenm.201601043

Table 1. Structures of Li_2FeSiO_4 polymorphs. a) β_{II} structure in which all the tetrahedral points are in the same direction, perpendicular to the close-packed planes, and share only corners with each other; chains of LiO_4 along *a* and parallel to chains of alternating FeO_4 and SiO_4; b) γ_s structure, half tetrahedra pointing in opposite directions and containing pairs of LiO_4/FeO_4 and LiO_4/LiO_4 edge-sharing tetrahedra (inset), c) γ_{II} structure in which the tetrahedra are arranged in groups of three with the central tetrahedron pointing in the opposite direction to the outer two, with which it shares edges (inset), in γ_{II} the group of 3 edge-sharing tetrahedra consist of the sequence Li-Fe-Li (inset). SiO_4 (yellow); FeO_4 (brown); LiO_4 (blue); light and dark blue tetrahedra represent crystallographically distinct Li sites.

Polymorph name	β_{II}	γ_S	γ_{II}
Annealing temperature [°C]	200	700	900
Crystallographic group	$Pmn2_1$	$P2_1/n$	$Pmnb$
Crystallographic representation	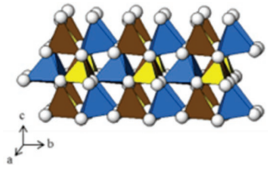	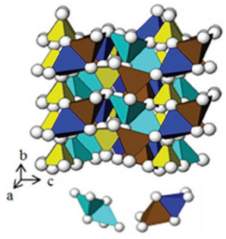	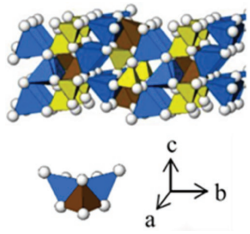

analysis performed by inductively coupled plasma mass spectroscopy (ICP-MS) showed that the expected stoichiometry was obtained for each sample to be within 2%. The X-ray diffraction (XRD) pattern of the Li_2FeSiO_4 shown in Figure 2a indicates that a pure material with a γ_S structure was obtained, as we have reported previously.[25] However, as x increased significant changes in the peaks between 39° and 44° 2θ (Fe Kα_1 radiation) were observed (Figure 2b); this region is particularly sensitive to the different polymorphs present in the material.[14] The small reflection occurring at around 40° 2θ is unique to the γ_S polymorph, being absent from the patterns of both β_{II} and γ_{II} forms (see Figure 2). Furthermore, the presence of three peaks between 41° and 43° 2θ is characteristic of the γ_{II} form. Hence, for low values of x in $Li_{2+2x}Fe_{1-x}SiO_4$ the powder diffraction patterns indicate the presence of a significant amount of the γ_S polymorph, while for higher levels of lithium excess the peak at 40° 2θ is absent and the diagnostic three reflections from the γ_{II} form are observed.

To obtain accurate values for phase fractions we used neutron diffraction data shown in Figure S1 (Supporting Information). No impurity such as Li_2SiO_3 or Fe_2O_3 was detected by neutron diffraction data for the range of compositions presented here, $0 \le x \le 0.3$. Corresponding refined crystallographic parameters are shown in Table S1 (Supporting Information). Rietveld refinement of the powder neutron diffraction data confirmed the presence of the two lithium iron silicate phases, the ratio of which changes as a function of x, as reported in **Table 2**. Different phases were tested and it was concluded unambiguously that no orthorhombic phase was present despite few reports in the literature.[50]

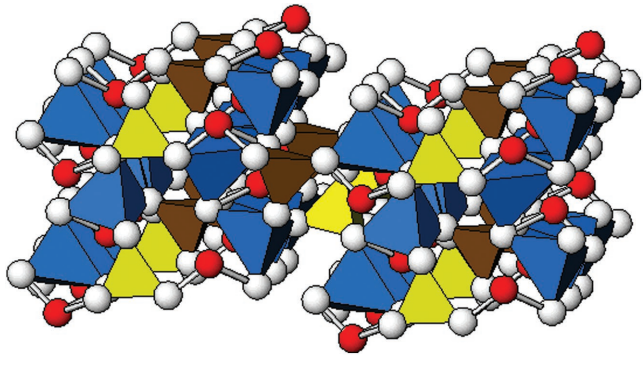

Figure 1. Lithium superionic conductor (LISICON) structure. $Si(Ge)O_4$ (yellow), MO_4 (brown), LiO_4 (blue), interstitial Li (red spheres).

Consistent with the qualitative examination of the XRD peaks, the γ_{II} form is seen to increase in phase content with x and when $x = 0.3$ no γ_S can be resolved. Profile fits to the data are shown in Figure S1 (Supporting Information) with refined parameters in Table S1 (Supporting Information). It should be noted that it was difficult to refine any lithium in the interstitial sites (an issue which is discussed in more detail later in the manuscript); however, the triggered phase transition does indicate a structural change. Given that the target of this work was to examine the performance of γ_{II} with interstitials ($Li_{2+2x}Fe_{1-x}SiO_4$) in comparison to the stoichiometric (Li_2FeSiO_4), all further studies will focus, for simplicity, on comparisons of $x = 0$ and $x = 0.3$ due to the sample purity.

Additionally, particle size analysis (Figure S2, Supporting Information) indicates that the two samples have a similar distribution (0.3–100 µm) with peaks at ≈30 µm. Scanning electron microscopy (SEM) images of the morphology corroborate this observation (Figure S2, Supporting Information). This suggests that any differences in kinetic behavior should not originate from different morphology or particle size. Characterization of similar materials by transmissison electron microscopy (TEM) can be found in refs. [57,58]

2.2. Electrochemical Studies

Since kinetic enhancements were of major concern in this study, electrodes were consistently prepared with a thickness of ≈20 µm such that lithium ion mass transport in the electrolyte should not limit performance over the rates examined in this work.[59] In **Figure 3**a the first potential profile as a function of

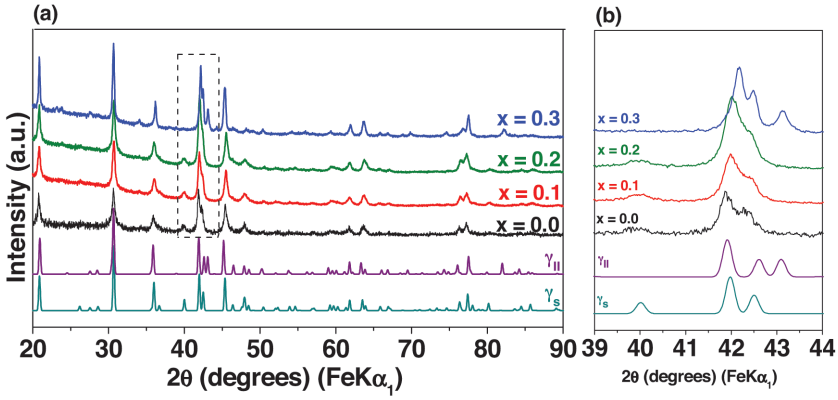

Figure 2. a) Powder X-ray diffraction patterns for the as-prepared $Li_{2+2x}Fe_{1-x}SiO_4$ materials ($0 \le x \le 0.3$) and reference patterns for Li_2FeSiO_4 in the $P2_1/n$ (γ_S) and $Pmnb$ (γ_{II}) space groups. b) XRD patterns in the selected region of 39°–44° 2θ.

capacity for γs Li_2FeSiO_4 is shown. The characteristic feature for this material is seen with a relatively flat plateau at around 3.2 V, identical to that reported by other authors who confirmed by XRD that the mechanism corresponds to a two-phase reaction on the first charge.[45] Over subsequent cycles a gradual voltage drop occurs, which results in a stable flat pseudoplateau cycling performance around 2.75 V (Figure 3b), as observed recently by Lu et al.[50] We believe this behavior corresponds to a transformation from the γ_S form to an inverse β_{II} structure,[14] although the nature of the phase transition has been shown to be dependent on cycling conditions, as has been observed with other systems.[30,50]

When Li was electrochemically de- and reintercalated into the γ_{II} $Li_{2.6}Fe_{0.7}SiO_4$ using the same potential window as used for the Li_2FeSiO_4 (Figure S3, Supporting Information) a second feature in the voltage profile could be observed on discharge taking place near the limiting voltage of 2 V. It appears likely that this low voltage process arises from the extraction and reinsertion of interstitial lithium ions (confirmed later by atomistic modeling results). It is unexpected that this low voltage feature should only appear on discharge as the interstitial lithium ions should be present in the pristine material. Given that this reaction appears to take place below 2.8 V it is likely that the material has been oxidized by exposure to the air[60] and results in the extraction of the lithium at this low voltage. In order to confirm that the low voltage behavior could be attributed to the interstitial lithium ions, a cell was discharged to 1.5 V versus Li^+/Li. Powder neutron diffraction data were then obtained on this discharged material, whose refined composition was $Li_{2.5}Fe_{0.75}SiO4$. Examination of data collected at longer

Table 2. Phase percentage of different polymorphs as a function of the value of x in $Li_{2+2x}Fe_{1-x}SiO_4$ obtained from Rietveld refinements against neutron data.

	γ_S [%]	γ_{II} [%]
$x \le 0$	100	–
$x = 0.1$	87	13
$x = 0.2$	57	43
$x = 0.3$	–	100

d-spacing (Bank 3 on Polaris, 52°) (**Figure 4**) shows clear evidence of an intense reflection around 4.9 Å that cannot be indexed using the γ_{II} unit cell. The peak can be indexed on the basis of a doubling of the unit cell along *a* (21 Å repeat). This was best described in the monoclinic space group $P2_1/m$, although the structure remains metrically orthorhombic. Refined parameters are shown in Table S2 (Supporting Information).

A combination of different Fourier methods, testing of interstitial sites derived from the LISICON structure together with those predicted by computation, enabled identification of an interstitial Li site (Li5) in distorted octahedral sites. The location of the interstitial sites is consistent with those seen in LISICON as shown in Figure 1.

Therefore, it was necessary to first discharge these materials to 1.5 V prior to a delithiation to 3.7 V to get a true representation of the behavior of the material. As shown in Figure 3c, the cycling performance for $Li_{2.6}Fe_{0.7}SiO_4$ shows that during the initial lithiation to 1.5 V a new sloping potential feature is observed centered around 2.2 V. The capacity of this feature is ≈33 mA h g^{-1} (Figure 3c), which corresponds well with the 37.7 mA h g^{-1} anticipated from the number of lithium interstitials (≈0.3). On delithiation of the material to a potential limit of 3.7 V the sloping region at 2.2 V is again observed along with a potential plateau at 3.1 V corresponding to the extraction of lithium from the tetrahedral sites within the $Li_{2.6}Fe_{0.7}SiO_4$. On discharge, a similar performance was observed. After ten cycles the high voltage plateau had faded to around 2.7 V, which is similar to the behavior seen for Li_2FeSiO_4 described earlier.[25] However, the potential of the interstitial sites remains almost unchanged with the same sloped plateau region seen at around 2 V. (For comparison, the pristine Li_2FeSiO_4 material was cycled between 1.5 and 3.7 V and is shown in Figure S4 (Supporting Information), where detrimental effects to the cycling performance were observed.)

Calculations related to the theoretical capacity are detailed in Table S4 (Supporting Information). The percentage of theoretical capacity obtained at a series of different rates is shown for both the Li_2FeSiO_4 and $Li_{2.6}Fe_{0.7}SiO_4$ materials in **Figure 5**.

Corresponding load curves at the tenth cycle are provided in Figure S6 (Supporting Information). In the case of $Li_{2.6}Fe_{0.7}SiO_4$ close to 100% of the theoretical capacity is extracted when the material is charged at around 10 mA g^{-1}. The capacity retention of the $x = 0.3$ sample is superior to the $x = 0$ sample for all the rates tested up to 1000 mA g^{-1}. Importantly, for the $Li_{2.6}Fe_{0.7}SiO_4$ sample a capacity of 70% of theoretical was achieved at rates as high as 1000 mA g^{-1} (≈8 C). This is consistent with improved ionic mobility of lithium within the material. In order to investigate the origin of this improvement further, load curves showing the first charge cycle at 10 and 500 mA g^{-1} for both the $x = 0$ and $x = 0.3$ samples are shown in **Figure 6**.

This graph clearly shows a significantly reduced overpotential at 500 mA g^{-1} in the $x = 0.3$ sample. This is particularly noticeable for the capacity extracted at lower potentials (in the 1.5–3 voltage range). This result supports the hypothesis that

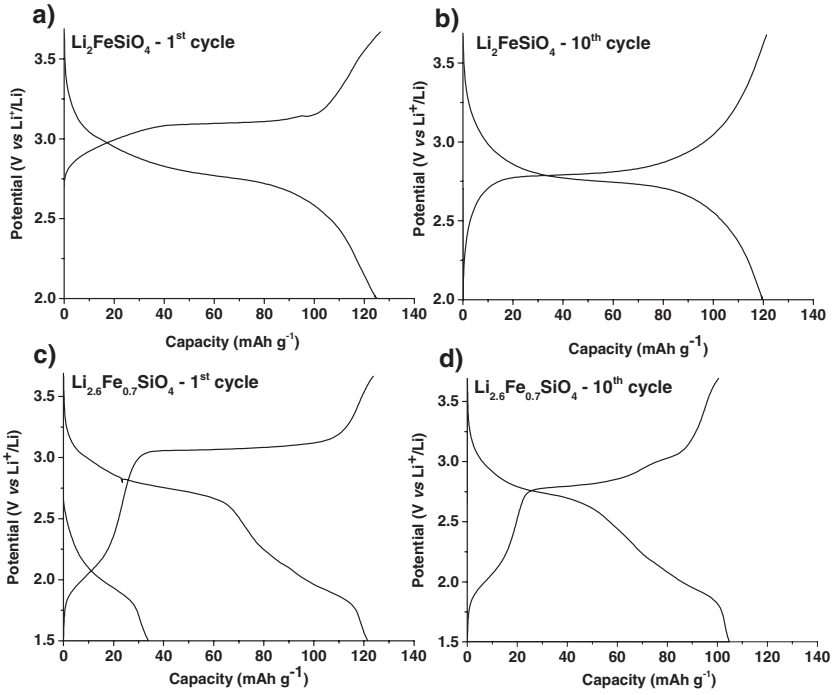

Figure 3. Load curves for as-prepared Li_2FeSiO_4 cycled between 2.0 and 3.7 V at 10 mA g^{-1} and 60 °C on the a) first cycle, and b) tenth cycle. Load curves for as-prepared $Li_{2.6}Fe_{0.7}SiO_4$ cycled between 1.5 and 3.7 V (starting with a discharge to insert Li interstitials) at 10 mA g^{-1} and 60 °C on the c) first cycle, and d) tenth cycle.

the interstitial lithium in these lithium-rich solid solutions exhibits greater mobility than the framework lithium (this result is probed further by the modeling work detailed below.)

To highlight further the excellent lithium mobility in the $Li_{2.6}Fe_{0.7}SiO_4$ material, we cycled the material only in this low voltage range which we believe to be related to the movement of fast lithium ions shown in **Figure 7**.

It can be seen that the overpotential required to extract the lithium was very low even at high rates leading to the conclusion that the interstitial lithium ions have high diffusion coefficients, which result from a similar effect to that seen in the LISICON-type materials, which exhibit high lithium-ion conductivity due to the presence of interstitial lithium in the structure.

The results shown in Figures 3, 5, 6, and 7 are all recorded at 60 °C, which is typically done to negate the problems caused by low conductivity. In order to test if the enhancements shown above improved the performance of room temperature cells, capacities at a series of different rates for both the Li_2FeSiO_4 and $Li_{2.6}Fe_{0.7}SiO_4$ are presented in **Figure 8**. It is clear that significantly improved capacities at all rates are seen for $Li_{2.6}Fe_{0.7}SiO_4$. These results show that by synthesizing materials containing interstitial lithium, the mobility of the Li ions in the electrode materials can be enhanced such that even room temperature cycling of these materials can be effectively performed. These results show that by designing modifications to the structure of materials through the addition of Li ions in previously vacant sites we can significantly enhance ionic mobility within silicate electrode materials.

2.3. Modeling of Structures and Lithium-Ion Transport

To fully understand the factors influencing the electrochemical behavior of the Li-rich silicate cathodes, it is clear that greater atomic-scale insights into the local structural and lithium transport properties are important, as highlighted by the recent work of Lu et al.[61,62] As noted, the lithium-rich $Li_{2+2x}Fe_{1-x}SiO_4$ adopts the γ_{II} structure including Li at tetrahedral framework sites and at interstitial sites with respect to Li_2FeSiO_4. For the atomistic simulations, numerous structural configurations of Li on framework and interstitial sites were first analyzed to find the low energy structure using multiple energy minimization calculations. The most favorable interstitial sites have octahedral coordination in accordance with the observed structure from powder neutron diffraction (Table S2, Supporting Information).

The Li^+ ions are found not to be randomly distributed over these octahedral sites. Instead, the simulated structure consists of many small regions or nanodomains of lithium-rich defect

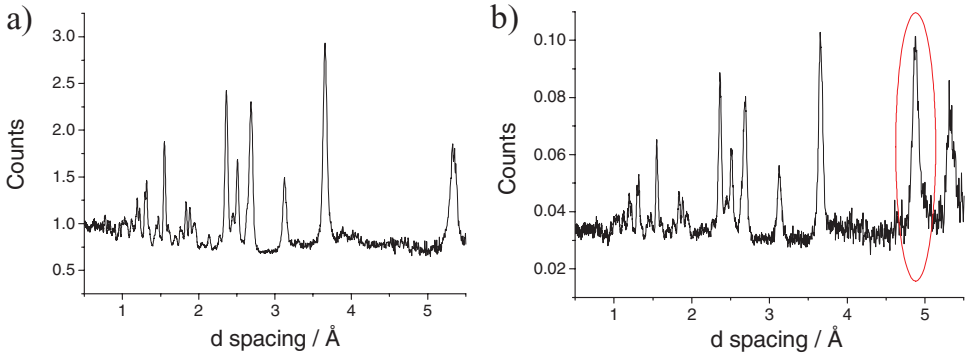

Figure 4. Powder neutron diffraction patterns (Polaris Bank 3) for a) as-prepared $Li_{2.6}Fe_{0.7}SiO_4$ and b) $Li_{2.6}Fe_{0.7}SiO_4$ discharged to 1.5 V with the superlattice reflection highlighted.

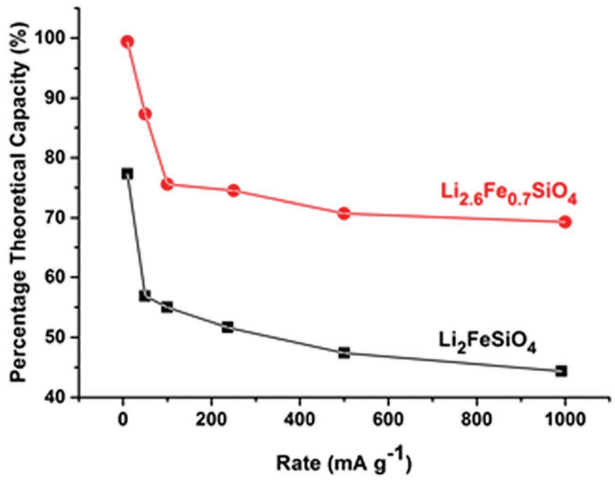

Figure 5. Percentage of theoretical capacity as a function of the discharge rate. Each capacity was determined from the first charge of a freshly assembled cell such that at the start of charge the Li_2FeSiO_4 was γ_s and $Li_{2.6}Fe_{0.7}SiO_4$ was γ_{ll}.

clusters. These defect clusters consist of typically three adjacent interstitial octahedrally coordinated lithium ions and neighboring tetrahedral lithium ions (illustrated in **Figure 9**) so that no Fe is present in the defect cluster. We note that similar lithium-rich defect clusters have been observed in the γ-structured $Li_3Zn_{0.5}GeO_4$ (LISICON) solid electrolyte, so that the entire structure of the solid consists of a mosaic of ordered substructures.[63]

To assess how the simulated structure compares with the observed crystal structure a list of calculated and experimental structural parameters of $Li_{2.6}Fe_{0.7}SiO_4$ is given in **Table 3**. The calculated unit cell parameters and bond lengths generally compare extremely well with those obtained experimentally. This reproduction of the complex structure gives us confidence that both the structural model and the interatomic potentials can be used reliably in the diffusion calculations (as shown in our previous simulation studies on electrode materials for lithium-ion batteries.[25,64–66])

A key feature of the experimental data is the sloping voltage behavior centered at ≈2.2 V observed during the initial stages of delithiation from 0–30 mA h g^{-1} in $Li_{2.6}Fe_{0.7}SiO_4$ (as shown in Figure 6). To assess this effect of the enrichment on the electrochemical properties we have compared the total energy after Li is removed from the octahedral and the tetrahedral sites. The calculations suggest that during the initial stages of delithiation, the octahedral lithium sites are depopulated before the tetrahedral sites.

To further understand the experimental observation of enhanced diffusion we used molecular dynamics (MD) techniques, which are well suited to probing Li^+ diffusion rates and mechanisms. First, the mean squared displacements (MSDs), $\langle[r(t)]^2\rangle$, of all lithium ions have been resolved and shown in **Figure 10**; the results show that lithium-ion diffusion is much higher in the Li-rich composition. The Li-ion diffusion coefficient (D_{Li}) can be derived from the MSD data, given by $D = (1/6t)\ \langle[r(t)]^2\rangle$. We calculate a D_{Li} value of 1.3×10^{-9} cm^2 s^{-1} for $Li_{2.6}Fe_{0.7}SiO_4$ at 473 K, which is three orders of magnitude higher than D_{Li} for stoichiometric Li_2FeSiO_4.

Accurate measurements of Li-ion diffusion coefficients for electrode materials are not straightforward and sometimes show significant scatter in values between different impedance studies. Nevertheless, experimental diffusion coefficients[31–33] for Li_2FeSiO_4 are found to be in the region of 10^{-12} to 10^{-11} cm^2 s^{-1}, which is consistent with our calculated value of 2×10^{-12} cm^2 s^{-1} at 473 K. Although there are currently no measured diffusion data for direct comparison for the Li-rich system, the magnitude is comparable to other cathode materials; for example, experimental diffusion coefficients of 10^{-8} to 10^{-11} cm^2 s^{-1} have been reported[67–71] for Li^+ diffusion in oxide cathodes such as $LiCoO_2$ and Li(Ni,Mn,Co)O_2. For the γ-phase solid electrolyte $Li_{2.5}Zn_{0.75}GeO_4$, Fujimura et al.[72] have calculated a D_{Li} of about 10^{-9} cm^2 s^{-1} at 500 K, which is in good agreement with our data for a similar LISICON structure.

Arrhenius plots (ln D versus $1/T$) for both $Li_{2.6}Fe_{0.7}SiO_4$ and Li_2FeSiO_4 are presented in **Figure 11**. Analysis of such data provides an estimate of the migration activation energy (E_{act}) using the standard Arrhenius relation

$$D = A \exp(-E_{act}/kT) \quad (1)$$

Migration activation energies of 0.37 and 0.84 eV are derived for $Li_{2.6}Fe_{0.7}SiO_4$ and Li_2FeSiO_4, respectively (for Li_2FeSiO_4, this is consistent with previous work[25,46–48,73]). These simulation results indicate much faster diffusion rates and lower migration energies for lithium-ions in $Li_{2+2x}Fe_{1-x}SiO_4$ cathode materials when interstitial lithium ions are present, which helps rationalize the observed enhancement in rate capability.

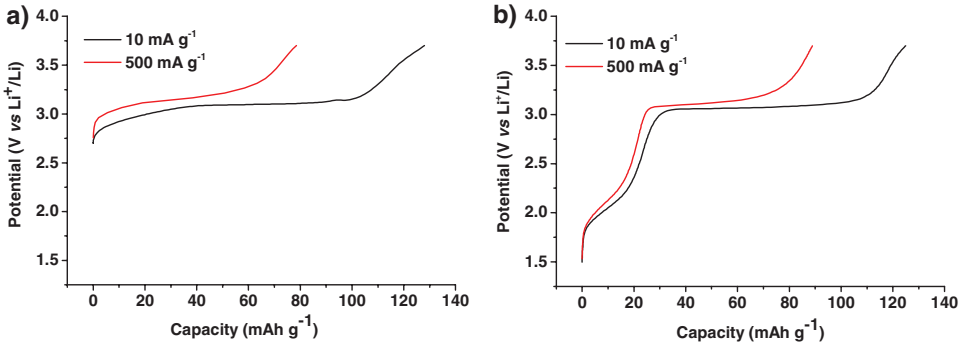

Figure 6. Load curves for a) Li_2FeSiO_4 and b) $Li_{2.6}Fe_{0.7}SiO_4$ obtained at 10 and 500 mA g^{-1} during the first cycle.

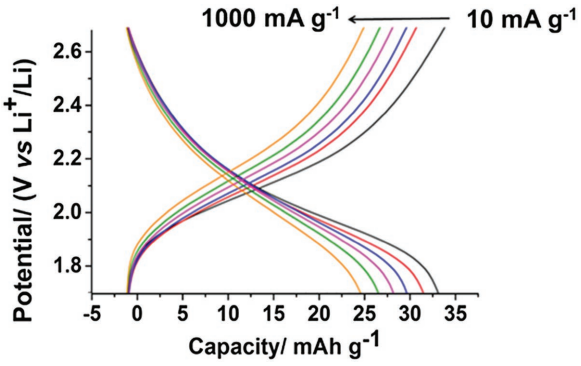

Figure 7. Load curves for $Li_{2.6}Fe_{0.7}SiO_4$ at 10 mA g^{-1} (—), 50 mA g^{-1} (—), 100 mA g^{-1} (—), 250 mA g^{-1} (—), 500 mA g^{-1} (—), and 1000 mA g^{-1} (—) between 1.5 and 2.7 V at 60 °C on the first cycle.

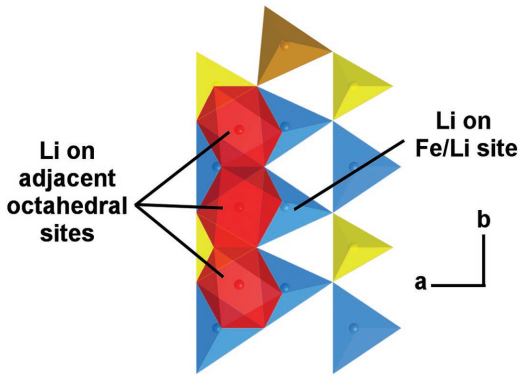

Figure 9. Typical lithium-rich defect cluster in $Li_{2.6}Fe_{0.7}SiO_4$, in which lithium occupies adjacent octahedral sites and shared Li/Fe tetrahedral sites. Octahedral interstitial Li ions are shown in red, tetrahedrally coordinated Li, Fe, and Si are shown in blue, brown, and yellow, respectively.

Given the stark difference in activation energies and diffusion coefficients it is possible that a significantly different diffusion mechanism is in operation in the Li-rich compounds. To help visualize the ion migration pathways, lithium diffusion density plots for $Li_{2.6}Fe_{0.7}SiO_4$ are shown in **Figure 12**. These plots show the accumulated density of lithium ion trajectories over the MD simulation. The diffuse distribution and overlapping of different lithium positions indicate that lithium ions in both octahedral and tetrahedral sites are involved in the diffusion processes.

The dimensionality of the Li diffusion can have a major impact on the Li extraction rate. For example, LiFePO4 is a 1D conductor and the presence of blocking defects in the 1D channels has been found to severely impede the diffusion and the capacity.[74] For Li_2FeSiO_4 previous computational studies[40–48,73,75–77] have focused on the noncycled stoichiometric phases and found lithium migration to proceed via a conventional vacancy hop mechanism between tetrahedral sites along 2D pathways where the plane of SiO_4/FeO_4 tetrahedra form a barrier to 3D conduction. In $Li_{2.6}Fe_{0.7}SiO_4$ our analysis reveals that the presence of lithium on some of the Fe sites increases the available diffusion pathways and provides a 3D Li ion conduction network. Such diffusion behavior is important since it allows lithium access through all surfaces of the particles, irrespective of their crystallographic orientation, and would be less affected by defects that block conduction; these results emphasize the importance of modifying the structure for enhanced diffusion kinetics.

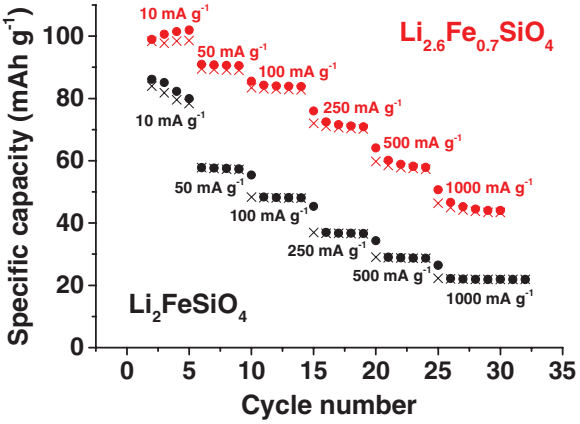

Figure 8. Charge and discharge capacities at a series of different rates for both Li_2FeSiO_4 and $Li_{2.6}Fe_{0.7}SiO_4$ at room temperature.

With regard to the atomistic mechanism, a key feature is that no direct lithium interstitial migration between octahedral sites is found. Instead, the MD results reveal that the lithium-rich defect cluster can migrate by a concerted knock-on movement of the Li^+ ions within the cluster, whereby octahedral interstitial Li^+ ions knock on Li^+ ions in face-sharing tetrahedral sites to unoccupied octahedral sites (illustrated in schematic form in **Figure 13**). As detailed previously,[78–80] a quantitative measure of concerted or cooperative migration can be gained through the Haven ratio, defined as the ratio of the tracer diffusion coefficient to a diffusion coefficient dependent on the ionic conductivity. A Haven ratio of 1.0 would suggest individual uncorrelated hopping events, whereas low values (<0.5) are observed in fast-ion conductors and other materials with highly correlated ionic diffusion.[78,79] For $Li_{2.6}Fe_{0.7}SiO_4$ the calculated Haven ratio is 0.38, which provides further support for the cooperative type mechanism that facilitates fast lithium-ion diffusion.

It is worth noting that similar cooperative mechanisms have been discussed in connection with interstitial lithium migration and defect cluster models in a group of solid electrolytes known as the gamma phases, of which $Li_{2+2x}Zn_{1-x}GeO_4$ (LISICON), $Li_{3+x}Ge_xV_{1-x}O_4$ and Li_3PO_4 are members,[63,67–71,81] but have not been widely examined in Li-rich electrode materials.

Table 3. Experimental and calculated structural parameters for $Li_{2.6}Fe_{0.7}SiO_4$.

Parameter	Calculated	Experimental
a b c [Å]	21.6643, 6.1830, 5.1657	21.3488, 6.2496, 5.0275
$\alpha\ \beta\ \gamma$ [°]	90.0, 90.12, 90.0	90.0, 90.06, 90.0
Mean Li–O [Å]	2.075	1.996
Mean Fe–O [Å]	1.980	2.014

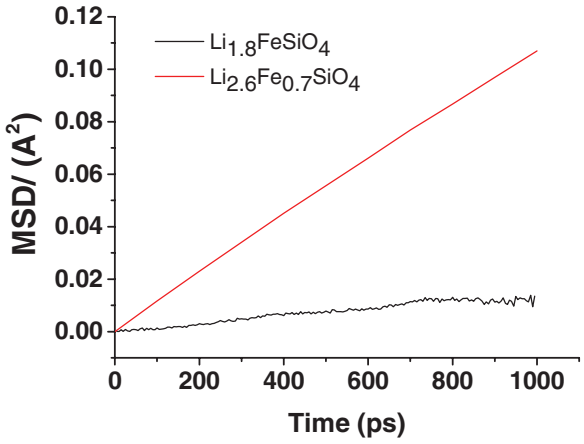

Figure 10. Mean squared displacement (MSD) of lithium ions versus time at 573 K comparing $Li_{2.6}Fe_{0.7}SiO_4$ to $Li_{2-x}FeSiO_4$ [$x = 0.2$]. The total simulation time was 3 ns and the final 1 ns is shown here.

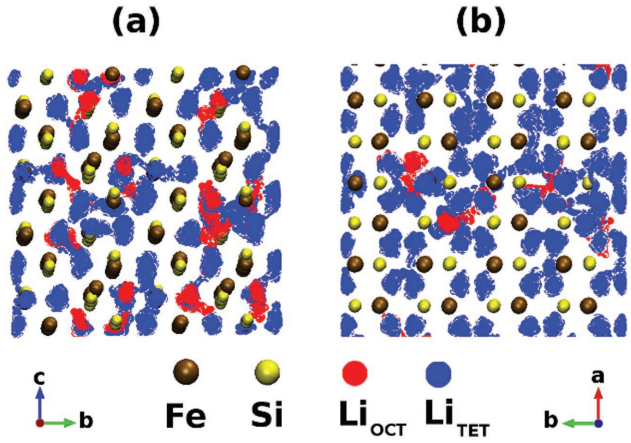

Figure 12. Lithium scatter plot for $Li_{2.6}Fe_{0.7}SiO_4$ collected over 1 ns of simulated time viewed in the a) *a–b* and b) *b–c* planes. Key: Fe (brown), Si (yellow), Li initially on tetrahedral sites (blue), and Li initially on octahedral interstitial sites (red).

3. Conclusion

It has been demonstrated experimentally and computationally that the Li^+ diffusivity and hence kinetics of stoichiometric silicate intercalation electrodes is slow. However, formation of Li-rich solid solutions such as $Li_{2+2x}Fe_{1-x}SiO_4$ (with $0 \le x \le 0.3$) can enhance the Li^+ diffusivity and kinetics by at least two orders of magnitude.

Neutron diffraction and atomistic modeling reveal that the location of the additional Li^+ is on interstitial octahedral sites. Electrochemical measurements show that for Li-rich $Li_{2.6}Fe_{0.7}SiO_4$ a capacity of 70% of theoretical was achieved at rates as high as 1000 mA g^{-1} (≈8 C) and that the overpotential required to extract the lithium was very low even at high rates; these results are consistent with enhanced lithium-ion mobility, and are similar to effects found for LISICON-type electrolytes, which exhibit high ion conductivity due to the presence of interstitial lithium. The computational MD results show that the enhanced Li^+ diffusivity in the Li-rich silicates is through a 3D conduction network. Furthermore, the Li^+ ions are not randomly distributed in the simulated structure, but comprised of nanodomains of lithium-rich clusters of neighboring octahedral interstitial lithium ions and tetrahedral lithium ions.

The key insights presented here help to rationalize the observed enhancement in rate performance of Li-rich silicate electrodes. Furthermore, they provide valuable understanding about how ion transport and hence kinetics can be enhanced that will inform the design and synthesis of future lithium intercalation materials.

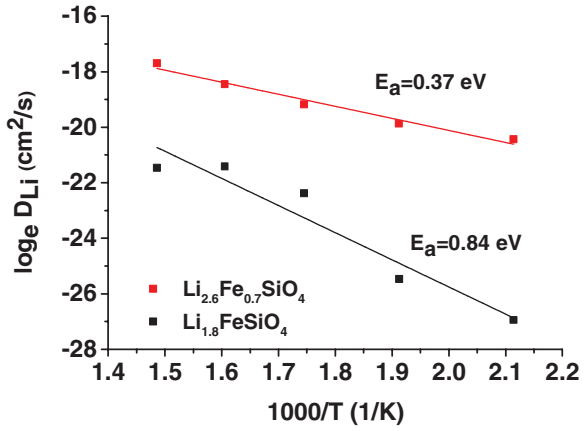

Figure 11. Arrhenius plot of lithium diffusion coefficients D_{Li} of $Li_{2-x}FeSiO_4$ ($x = 0.2$) and $Li_{2.6}Fe_{0.7}SiO_4$ with derived activation barriers (E_a).

4. Experimental Section

Experimental Techniques: A series of lithium-rich $Li_{2+2x}Fe_{1-x}SiO_4$ compounds ($0 \le x \le 0.3$) was prepared using the hydrothermal assisted gel synthesis method first described by Gong et al.[20] Iron (II) acetate (Strem), lithium acetate (Aldrich), and tetraethyl orthosilicate (Aldrich)

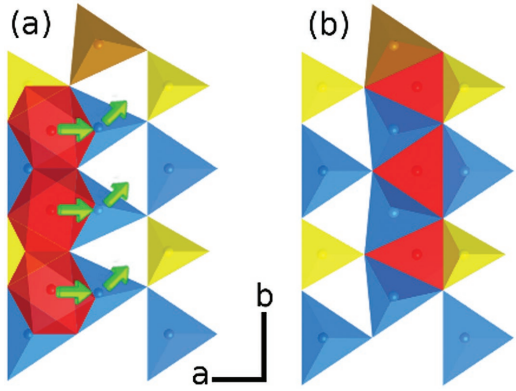

Figure 13. Transport mechanism of the Li-rich cluster in $Li_{2.6}Fe_{0.7}SiO_4$; a) initial configuration and b) after migration. Key: octahedral interstitial Li ions (red), tetrahedrally coordinated Li (blue), Fe (brown), and Si (yellow). Arrows indicate the migration pathways of lithium ions between face-sharing octahedral and tetrahedral sites via a cooperative knock-on mechanism.

were stirred for 45 min in ethanol together with 1.5 mL of acetic acid. The solution was then transferred to a Teflon-lined autoclave (45 mL), which was heated at 130 °C for 12 h. The resulting gel was dried at 100 °C, then mixed with sucrose (10 wt%), and ballmilled with 10 mL of acetone for 30 min. Following evaporation of the acetone, the sample was pelletized and calcined under flowing Argon at 650 °C for 3 h. All subsequent handling was carried out in an Ar-filled glove box (oxygen and water levels <1 ppm) as a precaution given the unknown sensitivity of these new samples to oxygen and moisture.

Powder X-ray diffraction data were collected on a Stoe STADI/P diffractometer operating in transmission mode with FeKα_1 radiation ($\lambda = 1.936$ Å) to eliminate Fe fluorescence.

Composite electrodes ($Li_{2+2x}Fe_{1-x}SiO_4$, Super S carbon and Kynar Flex 2801 [a copolymer based on polyvinylidene fluoride, PVDF] as binder, with weight ratios 80:10:10), were prepared by casting using the doctor blade technique. The mixture was first prepared as a slurry in *N*-methyl 2-pyrrolidinone and spread on to aluminum foil in an Ar-filled glovebox. These electrodes were then incorporated into electrochemical cells with a lithium metal (Aldrich) counter electrode and LP40 electrolyte (Merck, 1 M $LiPF_6$ in 1:1 vol/vol ethylene carbonate:diethyl carbonate). Electrochemical measurements were carried out at 30 and 60 °C in two electrode coin cells with Li counter/reference using a Maccor Series 4200 battery cycler.

Time-of-flight powder neutron diffraction data were obtained on the Polaris and GEM instruments at ISIS at the Rutherford Appleton Laboratory. Since lithium is a neutron absorber the data for as-prepared materials were corrected for absorption. The structures were refined by the Rietveld method using the program TOPAS Academic.[82] Powder neutron diffraction data were also obtained on an $Li_{2.6}Fe_{0.7}SiO_4$ sample discharged to 1.5 V versus Li^+/Li. The electrode was removed, washed with dry dimethyl carbonate, and dry tetrahydrofuran (THF) and dried by evaporation. The resulting powder was then transferred to a 2 mm quartz capillary and sealed.

Inductively coupled plasma mass spectroscopy and X-ray fluorescence were performed to confirm the chemical composition of the materials.

Particle size analysis by laser diffraction was performed on a Malvern Mastersizer, while SEM images were obtained using a Zeiss Merlin in secondary electron mode.

Atomistic Modeling: This study employed interatomic-potential-based simulation methods, which are well established and detailed elsewhere,[83–85] including a recent review on lithium battery materials.[64] The interatomic forces were treated by Buckingham potentials with parameters fitted simultaneously to all of the known polymorphs of Li_2FeSiO_4 (Table S2, Supporting Information). The position of the interstitial sites was examined by a screening process using a 0.1 Å grid of points using the GULP code.[84] For finite temperature lithium diffusion calculations, MD methods were used (DL-POLY[85]) with an NPT Berendsen ensemble and a timestep of 1 fs for MD runs of about 3 ns with supercells containing over 3500 atoms for good statistics. Such MD computational methods had been applied successfully to other Li-ion battery materials.[64–66,80,86]

Supporting Information

Supporting Information is available from the Wiley Online Library or from the author.

Research data has been deposited in ORA-data at DOI: 10.5287/bodleian:VjA9kpErd.

Acknowledgements

Financial support from the EPSRC Supergen Energy Storage Consortium (EP/L019469/1) and the Energy Materials Programme Grant (EP/K016288) is gratefully acknowledged. The membership in the UK's HPC Materials Chemistry Consortium (EP/L000202) allowed the use of the ARCHER computing facilities. The authors would like to thank Dr. P. Landon (Sasol Technology (UK) Ltd) for obtaining the variable temperature X-ray diffraction data.

Received: May 18, 2016
Revised: November 11, 2016
Published online: January 17, 2017

[1] A. Nyten, A. Abouimrane, M. Armand, T. Gustafsson, J. Thomas, *Electrochem. Commun.* **2005**, *7*, 156.
[2] M. S. Islam, R. Dominko, C. Masquelier, C. Sirisopanaporn, A. R. Armstrong, P. G. Bruce, *J. Mater. Chem.* **2011**, *21*, 9811.
[3] Z. L. Gong, Y. X. Li, Y. Yang, *Electrochem. Solid-State Lett.* **2006**, *9*, A542.
[4] D. Ensling, M. Stjerndahl, A. Nytén, T. Gustafsson, J. O. Thomas, *J. Mater. Chem.* **2008**, *19*, 82.
[5] K. Zaghib, a. Aitsalah, N. Ravet, A. Mauger, F. Gendron, C. Julien, *J. Power Sources* **2006**, *160*, 1381.
[6] S. Nishimura, S. Hayase, R. Kanno, M. Yashima, N. Nakayama, A. Yamada, *J. Am. Chem. Soc.* **2008**, *130*, 13212.
[7] R. Dominko, M. Bele, M. Gaberšček, A. Meden, M. Remškar, J. Jamnik, *Electrochem. Commun.* **2006**, *8*, 217.
[8] A. Kokalj, R. Dominko, G. Mali, A. Meden, M. Gaberscek, J. Jamnik, *Chem. Mater.* **2007**, *19*, 3633.
[9] R. Dominko, *J. Power Sources* **2008**, *184*, 462.
[10] M. Arroyo de Dompablo, M. Armand, J. Tarascon, U. Amador, *Electrochem. Commun.* **2006**, *8*, 1292.
[11] G. Mali, A. Meden, R. Dominko, *Chem. Commun.* **2010**, *46*, 3306.
[12] C. Sirisopanaporn, A. Boulineau, D. Hanzel, R. Dominko, B. Budic, A. R. Armstrong, P. G. Bruce, C. Masquelier, *Inorg. Chem.* **2010**, *49*, 7446.
[13] A. Boulineau, C. Sirisopanaporn, R. Dominko, A. R. Armstrong, P. G. Bruce, C. Masquelier, *Dalton Trans.* **2010**, *39*, 6310.
[14] C. Sirisopanaporn, C. Masquelier, P. G. Bruce, A. R. Armstrong, R. Dominko, *J. Am. Chem. Soc.* **2011**, *133*, 1263.
[15] R. J. Gummow, Y. He, *J. Power Sources* **2014**, *253*, 315.
[16] D. Rangappa, K. D. Murukanahally, T. Tomai, A. Unemoto, I. Honma, *Nano Lett.* **2012**, *12*, 1146.
[17] V. V. Politaev, A. A. Petrenko, V. B. Nalbandyan, B. S. Medvedev, E. S. Shvetsova, *J. Solid State Chem.* **2007**, *180*, 1045.
[18] L.-L. Zhang, S. Duan, X.-L. Yang, G. Liang, Y.-H. Huang, X.-Z. Cao, J. Yang, S.-B. Ni, M. Li, *Sci. Rep.* **2014**, *4*, 5064.
[19] S. Ferrari, D. Capsoni, S. Casino, M. Destro, C. Gerbaldi, M. Bini, *Phys. Chem. Chem. Phys.* **2014**, *16*, 10353.
[20] Z. L. Gong, Y. X. Li, G. N. He, J. Li, Y. Yang, *Electrochem. Solid-State Lett.* **2008**, *11*, A60.
[21] I. Belharouak, A. Abouimrane, K. Amine, *J. Phys. Chem. C* **2009**, *113*, 20733.
[22] T. Muraliganth, K. R. Stroukoff, A. Manthiram, *Chem. Mater.* **2010**, *22*, 5754.
[23] C. Lyness, B. Delobel, A. R. Armstrong, P. G. Bruce, *Chem. Commun.* **2007**, *46*, 4890.
[24] A. R. Armstrong, C. Lyness, M. Ménétrier, P. G. Bruce, *Chem. Mater.* **2010**, *22*, 1892.
[25] A. R. Armstrong, N. Kuganathan, M. S. Islam, P. G. Bruce, *J. Am. Chem. Soc.* **2011**, *133*, 13031.
[26] Z. Chen, S. Qiu, Y. Cao, J. Qian, X. Ai, K. Xie, X. Hong, H. Yang, *J. Mater. Chem. A* **2013**, *1*, 4988.
[27] G. He, G. Popov, L. F. Nazar, *Chem. Mater.* **2013**, *25*, 1024.
[28] R. Chen, R. Heinzmann, S. Mangold, V. S. K. Chakravadhanula, H. Hahn, S. Indris, *J. Phys. Chem. C* **2013**, *117*, 884.

[29] H. Zhu, X. Wu, L. Zan, Y. Zhang, *ACS Appl. Mater. Interfaces* **2014**, *6*, 11724.
[30] T. Masese, Y. Orikasa, C. Tassel, J. Kim, T. Minato, H. Arai, T. Mori, K. Yamamoto, Y. Kobayashi, H. Kageyama, Z. Ogumi, Y. Uchimoto, *Chem. Mater.* **2014**, *26*, 1380.
[31] L.-L. Zhang, S. Duan, X.-L. Yang, G. Peng, G. Liang, Y.-H. Huang, Y. Jiang, S.-B. Ni, M. Li, *ACS Appl. Mater. Interfaces* **2013**, *5*, 12304.
[32] L. Li, H. Guo, X. Li, Z. Wang, W. Peng, K. Xiang, X. Cao, *J. Power Sources* **2009**, *189*, 45.
[33] H. Gao, L. Wang, Y. Zhang, Y. Song, *Ionics (Kiel)*. **2013**, *20*, 817.
[34] M. Xie, R. Luo, R. Chen, F. Wu, T. Zhao, Q. Wang, L. Li, *ACS Appl. Mater. Interfaces* **2015**, *7*, 10779.
[35] T. Masese, C. Tassel, Y. Orikasa, Y. Koyama, H. Arai, N. Hayashi, J. Kim, T. Mori, K. Yamamoto, Y. Kobayashi, H. Kageyama, Z. Ogumi, Y. Uchimoto, *J. Phys. Chem. C* **2015**, *119*, 10206.
[36] L.-L. Zhang, S. Duan, X.-L. Yang, G. Liang, Y.-H. Huang, X.-Z. Cao, J. Yang, M. Li, M. C. Croft, C. Lewis, *J. Power Sources* **2015**, *274*, 194.
[37] J. Yang, L. Hu, J. Zheng, D. He, L. Tian, S. Mu, F. Pan, *J. Mater. Chem. A* **2015**, *3*, 9601.
[38] A. W. Brownrigg, G. Mountjoy, A. V. Chadwick, M. Alfredsson, W. Bras, J. Billaud, A. R. Armstrong, P. G. Bruce, R. Dominko, E. M. Kelder, *J. Mater. Chem. A* **2015**, *3*, 7314.
[39] J. Yang, X. Kang, L. Hu, X. Gong, S. Mu, *J. Mater. Chem. A* **2014**, *2*, 6870.
[40] R. C. Longo, K. Xiong, S. KC, K. Cho, *Electrochim. Acta* **2014**, *121*, 434.
[41] A. Saracibar, A. Van der Ven, M. E. Arroyo-de Dompablo, *Chem. Mater.* **2012**, *24*, 495.
[42] C. Eames, A. R. Armstrong, P. G. Bruce, M. S. Islam, *Chem. Mater.* **2012**, *24*, 2155.
[43] P. Zhang, C. H. Hu, S. Q. Wu, Z. Z. Zhu, Y. Yang, *Phys. Chem. Chem. Phys.* **2012**, *14*, 7346.
[44] N. G. Hörmann, A. Groß, *J. Solid State Electrochem.* **2013**, *18*, 1401.
[45] D. Lv, J. Bai, P. Zhang, S. Wu, Y. Li, W. Wen, Z. Jiang, J. Mi, Z. Zhu, Y. Yang, *Chem. Mater.* **2013**, *25*, 2014.
[46] A. Liivat, J. O. Thomas, *Solid State Ionics* **2011**, *192*, 58.
[47] D. Su, H. Ahn, G. Wang, *Appl. Phys. Lett.* **2011**, *99*, 141909.
[48] R. B. Araujo, R. H. Scheicher, J. S. de Almeida, A. Ferreira da Silva, R. Ahuja, *Solid State Ionics* **2013**, *247–248*, 8.
[49] X. Zhao, S. Wu, X. Lv, M. C. Nguyen, C.-Z. Wang, Z. Lin, Z.-Z. Zhu, K.-M. Ho, *Sci. Rep.* **2015**, *5*, 15555.
[50] X. Lu, H. Wei, H.-C. Chiu, R. Gauvin, P. Hovington, A. Guerfi, K. Zaghib, G. P. Demopoulos, *Sci. Rep.* **2015**, *5*, 8599.
[51] Z. Arthur, H.-C. Chiu, X. Lu, N. Chen, V. Emond, K. Zaghib, D.-T. Jiang, G. P. Demopoulos, *Chem. Commun.* **2015**, *52*, 190.
[52] L. Zhang, J. Ni, W. Wang, J. Guo, L. Li, *J. Mater. Chem. A* **2015**, *3*, 11782.
[53] V. Ramar, P. Balaya, *J. Power Sources* **2016**, *306*, 552.
[54] L. Qu, D. Luo, S. Fang, Y. Liu, L. Yang, S. Hirano, C.-C. Yang, *J. Power Sources* **2016**, *307*, 69.
[55] G. He, A. Manthiram, *Adv. Funct. Mater.* **2014**, *24*, 5277.
[56] P. G. Bruce, A. R. West, *J. Solid State Chem.* **1982**, *44*, 354.
[57] M. Dahbi, S. Urbonaite, T. Gustafsson, *J. Power Sources* **2012**, *205*, 456.
[58] P. Zuo, T. Wang, G. Cheng, X. Cheng, C. Du, G. Yin, *RSC Adv.* **2012**, *2*, 6994.
[59] P. A. Johns, M. R. Roberts, Y. Wakizaka, J. H. Sanders, J. R. Owen, *Electrochem. Commun.* **2009**, *11*, 2089.
[60] C. Deng, S. Zhang, Y. Gao, B. Wu, L. Ma, Y. H. Sun, B. L. Fu, Q. Wu, F. L. Liu, *Electrochim. Acta* **2011**, *56*, 7327.
[61] X. Lu, H.-C. Chiu, K. H. Bevan, D.-T. Jiang, K. Zaghib, G. P. Demopoulos, *J. Power Sources* **2016**, *318*, 136.
[62] X. Lu, H.-C. Chiu, Z. Arthur, J. Zhou, J. Wang, N. Chen, D.-T. Jiang, K. Zaghib, G. P. Demopoulos, *J. Power Sources* **2016**, *329*, 355.
[63] P. P. G. Bruce, I. Abrahams, *J. Solid State Chem.* **1991**, *95*, 74.
[64] M. S. Islam, C. A. J. Fisher, *Chem. Soc. Rev.* **2014**, *43*, 185.
[65] P. M. Panchmatia, A. R. Armstrong, P. G. Bruce, M. S. Islam, *Phys. Chem. Chem. Phys.* **2014**, *16*, 21114.
[66] C. Eames, J. M. Clark, G. Rousse, J.-M. Tarascon, M. S. Islam, *Chem. Mater.* **2014**, *26*, 3672.
[67] W. C. West, J. Soler, M. C. Smart, B. V. Ratnakumar, S. Firdosy, V. Ravi, M. S. Anderson, J. Hrbacek, E. S. Lee, A. Manthiram, *J. Electrochem. Soc.* **2011**, *158*, A883.
[68] M. Gozu, K. Świerczek, J. Molenda, *J. Power Sources* **2009**, *194*, 38.
[69] K. M. Shaju, G. V. S. Rao, B. V. R. Chowdari, *J. Electrochem. Soc.* **2004**, *151*, A1324.
[70] M. Park, X. Zhang, M. Chung, G. B. Less, A. M. Sastry, *J. Power Sources* **2010**, *195*, 7904.
[71] P. Jeevan-Kumar, K. Jayanth-Babu, O. M. Hussain, C. M. Julien, *Ionics (Kiel)*. **2012**, *19*, 421.
[72] K. Fujimura, A. Seko, Y. Koyama, A. Kuwabara, I. Kishida, K. Shitara, C. A. J. Fisher, H. Moriwake, I. Tanaka, *Adv. Energy Mater.* **2013**, *3*, 980.
[73] R. B. Araujo, R. H. Scheicher, J. S. de Almeida, A. Ferreira da Silva, R. Ahuja, *Solid State Commun.* **2013**, *173*, 9.
[74] R. Malik, D. Burch, M. Bazant, G. Ceder, *Nano Lett.* **2010**, *10*, 4123.
[75] P. Larsson, R. Ahuja, A. Nytén, J. O. Thomas, A. Nyten, J. O. Thomas, *Electrochem. Commun.* **2006**, *8*, 797.
[76] S. Q. Wu, Z. Z. Zhu, Y. Yang, Z. F. Hou, *Comput. Mater. Sci.* **2009**, *44*, 1243.
[77] G. Zhong, Y. Li, P. Yan, Z. Liu, M. Xie, H. Lin, *J. Phys. Chem. C* **2010**, *114*, 3693.
[78] G. Murch, *Solid State Ionics* **1982**, *7*, 177.
[79] M. Spaeth, K. D. Kreuer, J. Maier, C. Cramer, *J. Solid State Chem.* **1999**, *148*, 169.
[80] Y. Deng, C. Eames, J.-N. Chotard, F. Lalère, V. Seznec, S. Emge, O. Pecher, C. P. Grey, C. Masquelier, M. S. Islam, *J. Am. Chem. Soc.* **2015**, *137*, 9136.
[81] Y. A. Du, N. A. W. Holzwarth, *J. Electrochem. Soc.* **2007**, *154*, A999.
[82] A. A. Coelho, *J. Appl. Cryst.* **2000**, *33*, 899.
[83] G. V. Lewis, C. R. A. Catlow, *J. Phys. C Solid State Phys.* **1985**, *18*, 1149.
[84] J. D. Gale, A. L. Rohl, *Mol. Simul.* **2003**, *29*, 291.
[85] I. T. Todorov, W. Smith, K. Trachenko, M. T. Dove, *J. Mater. Chem.* **2006**, *16*, 1911.
[86] A. R. Armstrong, C. Lyness, P. M. Panchmatia, M. S. Islam, P. G. Bruce, *Nat. Mater.* **2011**, *10*, 223.

